An investigation on the effect of latent heat on the hygrothermal performance of earth building materials

Leonardo Maria Lalicata *, Agostino Walter Bruno, Domenico Gallipoli

Università di Genova, Via Montallegro, 1, 16145 Genova (GE), Italy

ARTICLE INFO

ABSTRACT

A coupled finite element model has been developed to simulate heat and water transfer across earth walls, considering pore water phase changes and the associated latent heat fluxes. The adopted approach simplifies parametric analyses by expressing all material hygrothermal properties as functions of porosity and water retention characteristics. The model is used to assess the influence of pore water latent heat on the passive hygrothermal regulation provided by two infinite earth walls that enclose an idealised room exposed to an external cold, humid climate. The findings indicate that latent heat buffering by pore water in earth walls increases with greater relative humidity gradients between the outdoor and indoor environments. The low vapour diffusivity confines latent heat production to the outer cold wall region where pore vapour condenses. The condensed moisture then flows inward and re-evaporates in the inner region of the wall. Additionally, the phase changes of water crossing the wall interfaces contribute to latent heat buffering, thereby enhancing hygrothermal efficiency. The process of pore vapour condensation and liquid transport intensifies with higher volumetric capacity and diffusivity of liquid water, which in turn increase with greater porosity, steeper retention curves, and larger saturation levels. Hydraulic effusivity is defined as a function of the volumetric capacity and diffusivity of liquid water to measure latent heat exchanges. Large hydraulic effusivity values indicate a greater potential for latent heat buffering. Finally, when compared to conventional concrete walls, earth walls demonstrate considerably better hygrothermal performance, which is mostly attributed to greater latent heat exchanges.

1. Introduction

Earth has become an increasingly popular building material in recent decades, attracting the attention of construction stakeholders because of its low environmental footprint compared to conventional alternatives, such as concrete or fired bricks [1–17]. Earthen materials are excellent passive hygrothermal regulators with the potential to increase occupants comfort while reducing air conditioning needs [18–22]. To date, however, most laboratory or field studies about the hygrothermal inertia of earthen materials have provided qualitative rather than quantitative analyses [23–30]. Only a few studies have quantified the positive impact of latent heat buffering by pore water on hygrothermal comfort and energy efficiency [31] whereas a larger number have concentrated on the incorporation of energy-intensive phase change materials within earth structures [32,33]. Consequently, the natural heat exchanges associated with pore water evaporation and condensation remain underexplored and partially unexploited.

To address this gap of knowledge, Lalicata et al. [34] formulated a hygrothermal model that combines unsaturated soil theories with the thermodynamics of porous media. This approach is consistent with previous geotechnical studies that have adopted similar strategies to investigate evaporation processes in cement-bentonite mixtures and coarse-grained soils [35,36]. Compared to traditional formulations [12,19,37,38], however, the proposed model requires a reduced number of parameters while accounting for pore water phase changes and the associated fluxes of latent heat.

Lalicata et al. [34] showed that the moisture buffering value, *MBV* [39] of earth is mostly governed by i) the unsaturated permeability of the material depending on both the saturated permeability and water retention behaviour and ii) the sensitivity of moisture storage to relative humidity changes. However, while *MBV* is a good indicator of the earth ability to exchange moisture with the surrounding environment, it does not provide an accurate measure of thermal inertia. This is because thermal inertia is greatly influenced by the storage/release of latent heat

---

during pore water evaporation/condensation throughout the earth mass and cannot therefore be solely related to moisture exchanges at the earth boundary.

To further explore this aspect, the present paper presents a numerical model of an idealised space enclosed, on both sides, by two symmetrical infinite earth walls. Results show that hygrothermal exchanges with the outdoor environment induce a variation of temperature and relative humidity inside the indoor space from the initial condition up to the final equilibrium state. This variation is strongly influenced by the earth properties that govern pore water condensation/evaporation and, hence, latent heat exchanges. The study also demonstrates that traditional materials, such as concrete, have a significantly weaker capacity for passive regulation, which highlights the advantages of earth in naturally controlling indoor temperature and humidity.

2. Hygrothermal coupled model

The earth is here modelled as a rigid three-phase porous medium consisting of soil grains (solid phase), water (in both liquid and gas phases) and dry air (in gas phase). The study also assumes that the resistance of the porous medium to gas flow is negligible and that the gas pressure is therefore always equal to the atmospheric value. The hygrothermal behaviour of the earth is thus analysed by simultaneously solving the two balance equations of water mass and thermal energy, which are coupled because both moisture and heat fluxes depend on the gradients of relative humidity and temperature. Previous work by the same research group [34] has also demonstrated that the change of pore vapour mass over time and the dependency of suction on temperature can be safely neglected in standard models without losing accuracy. This simplification is here retained to focus on the most important terms of the governing equations and to reduce potential sources of error.

2.1. Definition of earth state variables

The model assumes pure pore water (i.e. zero osmotic potential) and neglects moisture retention hysteresis. Under these hypotheses, the hydraulic state of the material can be alternatively defined in terms of degree of saturation S_l (−), gravimetric water content w_l (−), relative humidity h_r (−), matric suction s (MPa), partial vapour pressure p_v (kPa) or partial vapour density ρ_v (kg/m^3). These alternative variables are uniquely linked to each other by phase equations, constitutive relationships and thermodynamic laws, so any of them can describe the hydraulic state of the material.

The gravimetric water content w_l (−) and the degree of saturation S_l (−) are linked by the following phase equations:

$$w_l = \frac{1}{G_s}\frac{n}{1-n}S_l \tag{1}$$

where n (−) is the earth porosity and G_s (−) is the specific gravity of the earth solids, which is defined as:

$$G_s = \frac{\rho_s}{\rho_l} \tag{2}$$

where ρ_l (kg/m^3) is the liquid water density (here assumed equal to 1000 kg/m^3) and ρ_s (kg/m^3) is the density of the solid phase.

Instead, the matric suction s (named just suction in the following for simplicity) is the difference between the pore air pressure p_a (MPa) and the pore water pressure p_l (MPa). Because the pore air pressure is assumed atmospheric (i.e. $p_a = 0$), the suction s coincides with the pore water pressure p_l changed of sign:

$$s = p_a - p_l = -p_l \tag{3}$$

The suction s is related to the degree of saturation S_l through a constitutive relationship, i.e. the water retention relationship, describing the capacity of a porous material to store/release moisture

upon changes of capillary state. This work adopts the well-known Van Genuchten water retention relationship [40]:

$$S_l = S_{res} + (1 - S_{res})S_e \tag{4a}$$

where S_{res} is the residual degree of saturation while S_e is the effective degree of saturation defined as:

$$S_e = \left(1 + \left(\frac{s}{P}\right)^N\right)^{-M} \tag{4b}$$

where P (MPa), N (−) and M (−) are model parameters.

The Van Genuchten retention relationship of Eq. (4) can also be recast in terms of the gravimetric water content w_l using Eq. (1). At a given temperature T (K) and in the absence of osmotic effects, the suction s is linked to the relative humidity h_r by the following thermodynamic law, known as Kelvin's equation:

$$s = -\rho_l \frac{R}{M_w} T \ln h_r \tag{5}$$

where R (8.314 J/(mol K)) is the perfect gas constant and M_w (0.018 kg/mol) is the molar mass of water. Eq. (5) implies that, under typical service conditions, suction s is more influenced by changes in relative humidity h_r than temperature T, particularly at higher humidity levels [41].

The partial vapour pressure p_v is defined in terms of the relative humidity h_r as:

$$p_v = h_r p_{sat} \tag{6}$$

where p_{sat} is the saturated vapour pressure, which depends on the temperature T (K) according to the empirical relationship:

$$p_{sat}(T) = 0.6108 \times 10^{7.5\frac{(T-273.15)}{(T-35.85)}} \tag{7}$$

Finally, the partial vapour density ρ_v is related to the partial vapour pressure p_v via the perfect gas law as:

$$\rho_v = \frac{M_w}{RT} p_v \tag{8}$$

Based on Eqs. (6) and (8), the relative humidity h_r can also be recast as:

$$h_r = \frac{\rho_v}{\rho_{sat}} \tag{9}$$

where ρ_v and ρ_{sat} are the partial vapour density and saturated vapour density, respectively.

The relative humidity h_r and temperature T are routinely measured in both laboratory tests and full-scale building applications. Because of this, they are chosen in this work as the hydraulic and thermal state variables, which are calculated by simultaneously solving the water mass and energy balance equations introduced in the next section.

2.2. Governing balance equations

2.2.1. Water mass balance

Under standard service conditions, the moisture flow across building walls is mostly horizontal and the pore water pressure gradient governs liquid transfer according to Darcy law, while the contribution of the gravitational gradient is negligible. Under this hypothesis, the conservation of water mass, in both liquid and gas (vapour) phases, is imposed by equating storage to net flux as:

$$\rho_l n \frac{\partial S_l}{\partial t} = -\nabla\left(\rho_l\left(-\frac{K_l}{\rho_l g}\nabla p_l\right) - D_v \nabla \rho_v\right) \tag{10}$$

On the left-hand side of Eq. (10), the storage of vapour is neglected, as previously stated, due to the much lower density of the gas phase

compared to the liquid one [34].

On the right-hand side of Eq. (10), the liquid flow is described by the generalised Darcy law (i.e. first gradient term) where the unsaturated permeability K_l (m/s) is defined as:

$$K_l = K_{sat} k_{rl} \tag{11}$$

In Eq. (11), k_{rl} (−) is the relative permeability function of the effective degree of saturation S_e [42]:

$$k_{rl} = \sqrt{S_e} \left[1 - \left(1 - S_e^{M^{-1}} \right)^M \right]^2 \tag{12a}$$

where M is the same parameter as in the Van Genuchten relationship of Eq. (4b), while the saturated permeability K_{sat} (m/s) depends on porosity n according to the power relationship of Ren et al. [43]:

$$K_{sat} = 10^{\left(3.2 \frac{n}{1-n} - 7 \right)}. \tag{12b}$$

On the right-hand side of Eq. (10), the vapour flow is instead described by Fick law (i.e. second gradient term), where:

$$D_v = D\tau \, n(1 - S_l) \tag{13}$$

is the vapour diffusivity (m²/s), which depends on the vapour diffusivity in free air D (m²/s) and the tortuosity tensor τ (−) scaled by the volumetric vapour fraction, $n(1 - S_l)$ [35]. The tortuosity tensor τ is here assumed isotropic and therefore coincides with the following scalar quantity according to Lai et al. [44]:

$$\tau = (n(1 - S_l))^{2/3} \tag{14a}$$

while the vapour diffusivity in free air D depends on the temperature T (K) according to Kimball et al. [45]:

$$D = 0.229 \times 10^{-4} \left[1 + \frac{T}{273} \right]^{1.75} \tag{14b}$$

2.2.2. Thermal energy balance

By neglecting the energy changes due to wetting/drying processes and assuming that temperature is always in equilibrium between phases, the conservation of thermal energy is imposed by equating storage to net flux as follows:

$$(\rho c_p)_{eq} \frac{\partial T}{\partial t} = -\nabla \cdot (-\lambda \nabla T) - L_v m_{\to v} \tag{15}$$

where the convective component of heat transfer has been disregarded due to the low moisture flow rate. On the left-hand side of Eq. (15), the volumetric heat capacity of the soil $(\rho c_p)_{eq}$ (kJ/(m³·K)) is calculated by averaging the contributions of the solid and liquid phases as:

$$(\rho c_p)_{eq} = (1 - n)\rho_s c_{p,s} + n S_l \rho_l c_{p,l} \tag{16}$$

where $c_{p,s}$ and $c_{p,l}$ (kJ/(kg·K)) are the mass heat capacities of solid grains and liquid water, respectively. In Eq. (16), the contribution of the gas phase is instead neglected because of the much lower density of this phase compared to the solid and liquid phases. The values of ρ_s and $c_{p,s}$ vary with soil type while the value of $c_{p,l}$ can be reasonably assumed constant and equal to 4.183 kJ/(kg·K) [46].

On the right-hand side of Eq. (15), the conductive heat flow is described by Fourier law (i.e. the gradient term) where the thermal conductivity λ (W/(m·K)) is calculated as a function of both the thermal conductivity of the dry material λ_d and the gravimetric water content w_l according to Losini et al. [47]:

$$\lambda = \lambda_d + b w_l \tag{17}$$

where b is a model parameter.

The dry thermal conductivity λ_d is in turn related to the dry density

$\rho_d = \rho_s(1 - n)$ according to the following empirical relationship by Cagnon et al. [48]:

$$\lambda_d = 5.6 \times 10^{-2} e^{(1.4 \times 10^{-3} \rho_d)} \tag{18}$$

Eq. (18) implicitly assumes that the influence of earth mineralogy on thermal conductivity is negligible compared to the influence of dry density.

The last term on the right-hand side of Eq. (15) is the latent heat sink/source due to pore water phase changes and is equal to the product of the water latent heat L_v (here taken equal to 2.5·10⁶ J/kg) by the evaporation/condensation rate $m_{\to v}$, which is evaluated from the liquid phase balance as:

$$-m_{\to v} = \rho_l n \frac{\partial S_l}{\partial t} + \nabla \cdot \left(\rho_l \left(-\frac{K_l}{\rho_l g} \nabla p_l \right) \right) \tag{19}$$

2.2.3. Coupled hygrothermal balance

The water mass balance of Eq. (10) and the thermal energy balance of Eq. (15) can finally be recast in terms of temperature T and relative humidity h_r by using Eqs. (1), (3), (4), (5), (6), (7), (8) and (19) as:

$$C_l \frac{\partial h_r}{\partial t} = -\nabla \cdot \left(-D_l \rho_l \nabla h_r + \left(-D_v \frac{M_w}{RT} \left(p_{sat} \nabla h_r + h_r \left(\frac{dp_{sat}}{dT} - \frac{p_{sat}}{T} \right) \nabla T \right) \right) \right) \tag{20}$$

$$(\rho c_p)_{eq} \frac{\partial T}{\partial t} = -\nabla \cdot (-\lambda \nabla T) + L_v \left(C_l \frac{\partial h_r}{\partial t} + \nabla \cdot (-D_l \rho_l \nabla h_r) \right) \tag{21}$$

where C_l (kg/m³) is the volumetric liquid water capacity defined as:

$$C_l = \rho_l n \frac{\partial S_l}{\partial h_r} \tag{22}$$

and D_l (m²/s) is the liquid water diffusivity defined as:

$$D_l = \frac{K_l}{g} \frac{R}{M_w} \frac{T}{h_r} \tag{23}$$

As mentioned earlier, the dependency of suction on temperature has been neglected in both Eqs. (20) and (21) because of its marginal influence on the results. Additional details are reported in Lalicata et al. [34].

3. Numerical model

The above system of two partial differential equations has been implemented in the Comsol Multiphysics finite element software to calculate the hygrothermal state of an idealised room of width $L_i = 5$m enclosed by two symmetrical earth walls of thickness $L_w = 0.4$m (Fig. 1a). The two walls extend infinitely in-plane and are exposed to fixed values of relative humidity and temperature on their outdoor faces. Due to symmetry and infinite extension of the walls, only half geometry is considered and the problem is modelled as a one-dimensional case. The wall is therefore discretised by a linear mesh while the idealised room is modelled as a single point due to the assumption of spatial uniformity of indoor humidity and temperature (Fig. 1b). This assumption is acceptable as the present work focuses on the hygro-thermal transport across the wall rather than on the indoor distribution of humidity and temperature. Therefore, in the absence of indoor sources/sinks of vapour and heat, the following two balance equations govern the variations of the relative humidity $h_{r,i}$ and temperature T_i inside the idealised room:

$$\frac{L_i}{2} \frac{M_w}{RT_i} \left(p_{sat}(T_i) \frac{\partial h_{r,i}}{\partial t} + h_{r,i} \left(\frac{dp_{sat}(T_i)}{dT_i} - \frac{p_{sat}(T_i)}{T_i} \right) \frac{\partial T_i}{\partial t} \right)$$
$$= \beta_i \left(p_{sat}(T_{if}) h_{r,if} - p_{sat}(T_i) h_{r,i} \right) \tag{24}$$
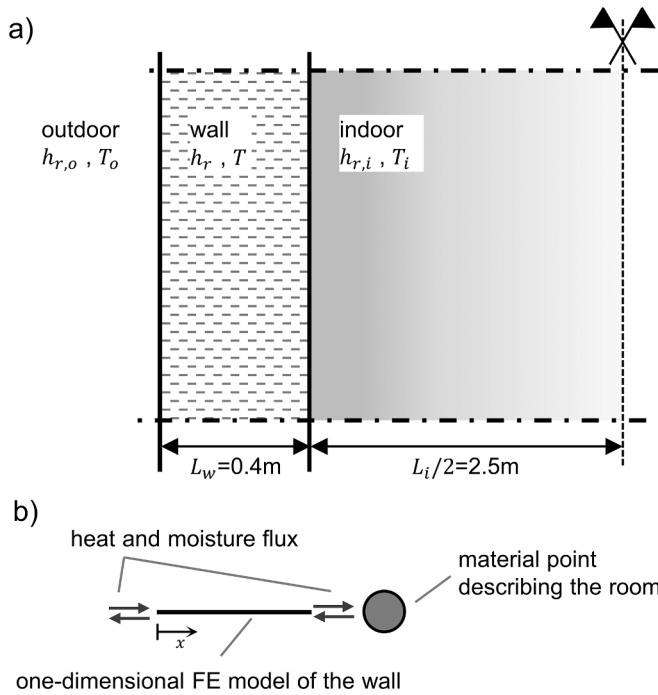
a)

b)

Fig. 1. a) Scheme of symmetric wall-room system (not to scale), b) one-dimensional numerical model.

$$\frac{L_i}{2}\frac{\partial T_i}{\partial t}\rho_i c_{p,i} = \alpha_i\left(T_{if} - T_i\right) \quad (25)$$

The left-hand sides of Eqs. (24) and (25) govern the storage of vapour and heat inside the room where ρ_i and $c_{p,i}$ are the density and mass heat capacity of the indoor air, which are respectively calculated as:

$$\rho_i = \rho_a X_a + \rho_v X_v \quad (26a)$$

$$c_{p,i} = \frac{\left(X_a M_a c_{p,a} + X_v M_w c_{p,v}\right)}{\left(X_a M_a + X_v M_w\right)} \quad (26b)$$

In Eq. (26), ρ_v (kg/m³), $X_v = \frac{p_{sat}}{p_{ref}}h_{r,i}$ (−), M_w (0.018 kg/mol) and $c_{p,v}$ (1.890 kJ/(kg·K)) are respectively the density (evaluated via Eq. (8)), the molar fraction at the reference pressure $p_{ref} = 1$ atm, the molar mass and the mass heat capacity of vapour, while $\rho_a = \frac{M_a}{RT}p_{ref}$ (kg/m³), $X_a = 1 - X_v$ (−), M_a (0.02897 kg/mol) and $c_{p,a}$ (1.005kJ/(kg·K)) are the same parameters for the dry air.

Conversely, the right-hand sides of Eqs. (24) and (25) describe the fluxes of moisture and heat across the wall boundary where $h_{r,if}$ and T_{if} are the relative humidity and temperature on the indoor wall face (which differ from the room values $h_{r,i}$ and T_i) while $\alpha_i = 8$ W/(m²K) and $\beta_i = 2.5 \times 10^{-8}$ kg/(m²sPa) are the indoor heat and vapour mass transfer coefficients [37].

The following hygrothermal boundary conditions are imposed on the indoor wall edge:

$$\begin{bmatrix} \left(\boldsymbol{g}_l + \boldsymbol{g}_v\right) \bullet \boldsymbol{n} \\ \left(\boldsymbol{g}_T - L_v\boldsymbol{g}_l\right) \bullet \boldsymbol{n} \end{bmatrix} = \begin{bmatrix} \beta_i\left(p_{sat}\left(T_{if}\right)h_{r,if} - p_{sat}\left(T_i\right)h_{r,i}\right) \\ \alpha_i\left(T_{if} - T_i\right) \end{bmatrix} \quad (27)$$

where $\boldsymbol{g}_l$, $\boldsymbol{g}_v$ and $\boldsymbol{g}_T$ are the liquid, vapour and heat fluxes, respectively, $\boldsymbol{n}$ is the unit vector normal to the wall face while the product $L_v\boldsymbol{g}_l$ accounts for the energy flux associated to phase changes at the wall edge. Eq. (27) is the conventional hygrothermal boundary condition adopted in building models [37] whereby moisture and heat transfers across the air-wall interface are proportional to the difference of the relevant driving variables via suitable transfer coefficients.

On the outdoor wall edge, the following boundary conditions are

similarly imposed:

$$\begin{bmatrix} \left(\boldsymbol{g}_l + \boldsymbol{g}_v\right) \bullet \boldsymbol{n} \\ \left(\boldsymbol{g}_T - L_v\boldsymbol{g}_l\right) \bullet \boldsymbol{n} \end{bmatrix} = \begin{bmatrix} \beta_o\left(p_{sat}\left(T_o\right)h_{r,o} - p_{sat}\left(T_{of}\right)h_{r,of}\right) \\ \alpha_o\left(T_o - T_{of}\right) \end{bmatrix} \quad (28)$$

where $\alpha_o = 23$ W/(m²K) and $\beta_o = 7.5 \times 10^{-8}$ kg/(m²sPa) are the outdoor heat and vapour mass transfer coefficients [37] while $h_{r,of}$ and T_{of} are the relative humidity and temperature on the outdoor wall face (which differ from the imposed external values $h_{r,o}$ and T_o).

The above numerical model can thus predict the temporal variation of relative humidity and temperature inside the room according to the imposed external conditions. The reference earth parameters are listed in Table 1 and have been determined from the experimental data of Soudani et al. [19].

Preliminary analyses, not reported here, have shown that the effect of pore water latent heat exchanges on the hygrothermal performance of earth walls is maximised when the outdoor and indoor values of relative humidity are significantly different, a scenario that typically occurs during cold and wet winters or hot and dry summers. The subsequent analysis will focus solely on the case of cold and wet winters, but similar conclusions can be drawn for the hot and dry summer scenario.

Preliminary analyses have also indicated that the daily fluctuations of outdoor relative humidity and temperature have a negligible impact on the hygrothermal response of the wall when compared to the effect of the average difference between outdoor and indoor values. Therefore, in the sake of simplicity, this work imposes constant outdoor values of relative humidity and temperature, equal to 0.80 and 8 °C, respectively, while the corresponding initial indoor values are 0.50 and 20 °C. The study also assumes that the initial values of relative humidity and temperature across the wall are identical to those of the indoor environment, i.e. 0.50 and 20 °C, respectively.

The results are presented in terms of changes of indoor relative humidity and temperature, calculated over a 50 day period leading to equilibrium with the imposed outdoor conditions. The hygrothermal impact of the pore water phase changes is highlighted by comparing two distinct cases with and without consideration of latent heat, i.e. with $L_v = 2.5 \times 10^6$ J/kg and $L_v = 0$, respectively.

4. Reference model results

Fig. 2 shows that, if latent heat is neglected, the room temperature drops from 20 °C to 8 °C after about one week, when it reaches thermal equilibrium with the external environment. Conversely, if latent heat is accounted for, the temperature reduces from 20 °C to 10.5 °C in about one week, then it remains stable for approximately 3 days before slowly reducing towards equilibrium at 8 °C. The hygrothermal activity of the earth therefore counteracts indoor heat losses maintaining a higher temperature (approximately +2.5 °C) for a longer time compared to the same material with zero latent heat.

Unlike temperature, Fig. 2 shows a virtually identical evolution of indoor relative humidity for both cases. This is because relative humidity is mostly governed by the hydraulic boundary conditions and is practically unaffected by exchanges of latent heat.

This advantageous hygrothermal behaviour can be explained by

Table 1
Reference parameter values of earth walls.

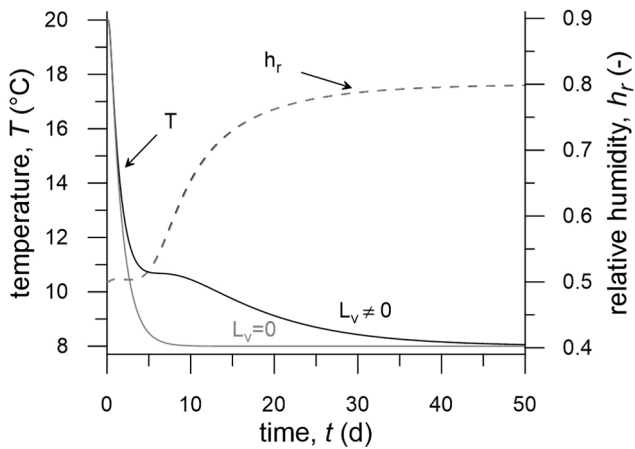| Parameter	Symbol	Value
Porosity (−)	n	0.35
Grains density (kg/m³)	ρ_s	2650
Van Genuchten parameter (MPa)	P	0.9
Van Genuchten parameter (−)	N	1.74
Van Genuchten parameter (−)	$M = 1 - 1/N$	0.42
Van Genuchten residual saturation (−)	S_{res}	0
Grains heat capacity (kJ/(kg·K))	$c_{p,s}$	0.648
Thermal conductivity parameter (W/(m·K))	b	9.22

Fig. 2. Influence of pore water latent heat exchanges in earth walls on the evolution of indoor relative humidity and temperature over time.

examining the specific latent heat fluxes (i.e. the latent heat fluxes per unit volume) across the wall thickness at different times. Fig. 3a shows that the specific latent heat fluxes are highest at earlier times when the wall hydraulic state is far from equilibrium, leading to significant pore water phase changes. Moisture penetration from the outside into the wall increases the relative humidity inside earth pores, surpassing equilibrium with the local pore suction. This imbalance results in water condensation and the consequent release of latent heat, as indicated by the positive fluxes of Fig. 3a. This heat generation is however restricted to the external wall layer because the low gas diffusivity limits the inward movement of vapour, thus preventing the condensation front from advancing deeper into the wall. This restriction is somewhat offset by the inward movement of condensed water, which partly restores the pore suction in the external earth layer, together with the associated potential for further condensation. The condensed water moves inward into the lower humidity regions of the wall where it reduces the local pore suction below equilibrium, causing evaporation and the consequent absorption of latent heat as indicated by the negative fluxes in Fig. 3a.

This ongoing mechanism of condensation followed by liquid transport helps to maintain a relative humidity differential between the external environment and the earth surface, which ensures the continued penetration of moisture according to the boundary condition of Eq. (28). Without such a mechanism, the humidity levels of the external environment and the earth surface would be very similar because of the small gas diffusivity, virtually eliminating the driving force for moisture penetration into the wall.

Fig. 3b shows the temporal evolution of the latent heat flux

contributions (per unit wall area) from the wall core and interfaces, respectively. The former contribution is calculated by integrating the curves of Fig. 3a across the wall thickness at different times while the latter one is calculated as the algebraic sum of the two boundary conditions of Eqs. (27) and (28) at the internal and external wall edges, where evaporation and condensation respectively take place. Fig. 3b indicates that, during the early stages of the simulation, the wall core generates (positive) latent heat as condensation in the outer region dominates. This situation however reverses after about 10 days when (negative) latent heat is removed as evaporation in the inner region takes over. The wall interfaces instead always produce (positive) latent heat, which decreases monotonically from a large initial value to about zero after 50 days.

Finally, Fig. 3b shows the total latent heat flux (per unit wall area), summing the above two contributions, which is always positive and peaks at about 15 W/m^2 after 2 days before gently decreasing towards zero. This significant generation of energy explains the delayed drop in room temperature for the case where latent heat is considered compared to the case where latent heat is neglected (Fig. 2).

5. Parametric study

The previous analysis has shown that the energy efficiency of earth walls depends not only on their thermal conductivity and volumetric heat capacity, but also on latent heat exchanges during condensation or evaporation of pore water. These exchanges increase when the volumetric liquid water capacity C_l of Eq. (22) and the liquid water diffusivity D_l of Eq. (23) are larger according to the previously described mechanism of condensation and liquid transport. To explore these aspects, this section examines the sensitivity of the indoor hygrothermal conditions when the porosity and water retention characteristics of the earth walls vary within realistic ranges [49–50].

Table 2 lists the earth hygrothermal properties calculated from the phase and constitutive relationships of Section 2 for different porosity values n while all other parameters are fixed at their reference values of Table 1. A larger porosity produces beneficial increases of volumetric liquid water capacity C_l, according to Eq. (22), and liquid water diffusivity D_l (due to growing saturated permeability K_l), according to Eqs. (11), (12) and (23), which result in growing exchanges of latent heat. A larger porosity also produces a beneficial reduction of thermal conductivity λ as the decrease of dry conductivity λ_d outweighs the growth of water content w_l, according to Eqs. (1), (17) and (18). On the other hand, an increase in porosity leads to a disadvantageous reduction in volumetric heat capacity $(\rho c_p)_{eq}$, according to Eq. (16). Finally, Table 2 indicates that the vapour diffusivity D_v increases with growing porosity one order of magnitude less than the liquid water diffusivity D_l.

Table 3 lists instead the earth hygrothermal properties calculated from the phase and constitutive relationships of Section 2 for different
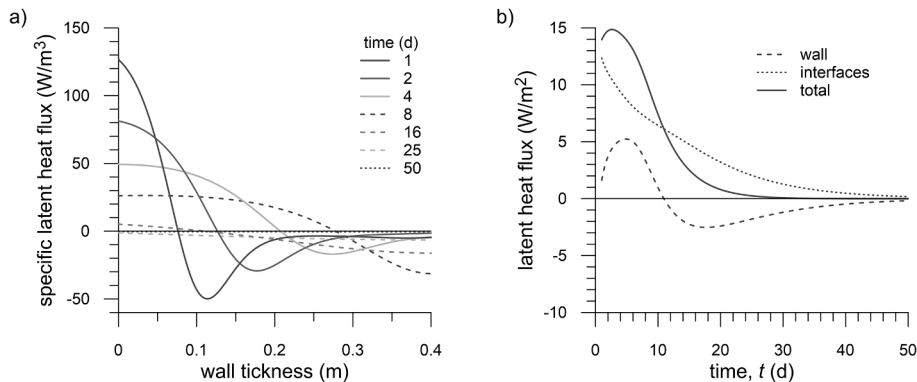

Fig. 3. Energy generation by water phase changes: a) distribution of specific latent heat fluxes across the wall core, b) contributions of wall core and interfaces to the total latent heat flux.

Table 2
Influence of porosity n on the hygrothermal properties of the earth.

Porosity	Dry density	Water content*	Volumetric liquid water capacity*	Volumetric heat capacity*	Liquid water diffusivity*	Vapour diffusivity*	Thermal conductivity*
n	ρ_d	w_l	C_l	$(\rho c_p)_{eq}$	D_l	D_v	λ
(−)	(kg/m³)	(−)	(kg/m³)	(kJ/(m³·K))	(m²/s)	(m²/s)	(W/(m·K))
0.15	2253	0.002	10.3	1480	3.1×10^{-11}	3.3×10^{-6}	1.33
0.2	2120	0.003	13.7	1401	5.3×10^{-11}	5.3×10^{-6}	1.12
0.25	1988	0.004	17.1	1321	9.9×10^{-11}	7.7×10^{-6}	0.94
0.3	1855	0.005	20.6	1242	2.0×10^{-10}	1.0×10^{-5}	0.80
0.35	1723	0.007	24.0	1163	4.5×10^{-10}	1.4×10^{-5}	0.68
0.4	1590	0.008	27.4	1084	1.2×10^{-9}	1.7×10^{-5}	0.59
0.45	1458	0.010	30.8	1005	3.5×10^{-9}	2.1×10^{-5}	0.52

* Computed at $h_r = 0.50$, $T = 20\ °C$.

Table 3
Influence of retention parameter N on the hygrothermal properties of the earth.

Retention parameter	Degree of saturation*	Water content*	Volumetric liquid water capacity*	Volumetric heat capacity*	Liquid water diffusivity*	Vapour diffusivity*	Thermal conductivity*
N	S_l	w_l	C_l	$(\rho c_p)_{eq}$	D_l	D_v	λ
(−)	(−)	(−)	(kg/m³)	(kJ/(m³·K))	(m²/s)	(m²/s)	(W/(m·K))
1.4	0.156	0.032	62.8	1344	1.0×10^{-8}	1.1×10^{-5}	0.92
1.5	0.098	0.020	49.4	1260	4.5×10^{-9}	1.2×10^{-5}	0.81
1.6	0.062	0.012	37.3	1206	1.8×10^{-9}	1.3×10^{-5}	0.74
1.7	0.039	0.008	27.3	1173	6.7×10^{-10}	1.3×10^{-5}	0.70
1.8	0.024	0.005	19.6	1152	2.4×10^{-10}	1.4×10^{-5}	0.67
1.9	0.015	0.003	13.9	1139	8.7×10^{-11}	1.4×10^{-5}	0.65
2	0.010	0.002	9.7	1130	3.0×10^{-11}	1.4×10^{-5}	0.64

* Computed at $h_r = 0.50$, $T = 20\ °C$.

values of the Van Genuchten parameter N while all other parameters are fixed at their reference values of Table 1. These values of N correspond to different retention curves, all falling within the bounds identified by Gallipoli et al. [50] as illustrated in Fig. 4 over the relative humidity interval from 0.3 to 0.8 (equivalent to a suction interval from 30 to 170 MPa), which is typical of building service conditions. The parameter N is inversely related to the slope of the retention curves in Fig. 4, meaning that a reduction in N produce an advantageous increase in volumetric liquid water capacity C_l, that is, a greater sensitivity of moisture content to relative humidity according to Eq. (22). A decrease of N also results in higher values of degree of saturation according to Eq. (4) and, hence, in a beneficial increase of liquid water diffusivity D_l according to Eqs. (11),

(12) and (23). Notably, higher values of C_l and D_l facilitate greater exchanges of latent heat as previously discussed. The higher saturation associated to decreasing values of N also result in a beneficial increase of volumetric heat capacity $(\rho c_p)_{eq}$ according to Eq. (16), but a disadvantageous increase of thermal conductivity λ, according to Eqs. (1) and (17). Finally, decreasing values of N produce negligible changes of the vapour diffusivity D_v, unlike the liquid water diffusivity D_l which instead varies by three orders of magnitude over the same range.

5.1. Effect of porosity n

Fig. 5 presents the temporal evolution of the thermal gain ΔT, i.e. the difference in indoor temperature between the two cases with $L_v \neq 0$ and
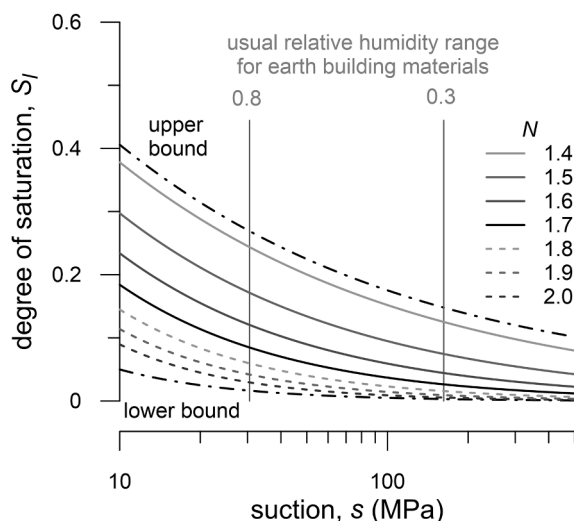
Fig. 4. Water retention curves investigated in this study.
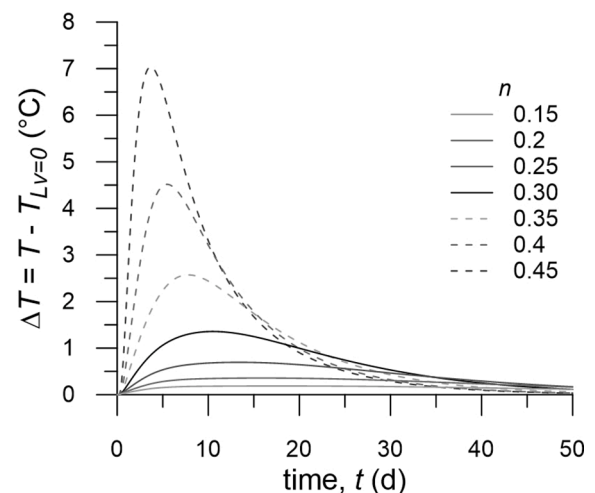
Fig. 5. Thermal gain over time for different values of porosity n.

$L_v = 0$, for different porosity values n while the remaining parameters are fixed at their reference values of Table 1. For a highly porous material with $n = 0.45$, the thermal gain peaks at about 7 °C after approximately 4 days, followed by a progressive reduction towards zero. In contrast, for a highly compacted material with $n = 0.15$, the hygrothermal performance is much poorer with a maximum thermal gain of only 0.2 °C, which remains approximately constant during the whole simulation period. These findings align with experimental data by Bruno et al. [28], who observed that a low porosity wall made of hypercompacted earth bricks exhibited a significantly poorer thermal performance compared to a high porosity one made of Proctor-compacted earth bricks.

Overall, the results in Fig. 5 can be explained by the threefold advantage of a larger porosity, leading to higher values of volumetric liquid water capacity C_l and liquid water diffusivity D_l, as well as lower values of thermal conductivity λ (Table 2). These positive effects significantly outweigh the adverse influence of the reducing volumetric heat capacity $(\rho c_p)_{eq}$ (Table 2).

5.2. Effect of retention parameter N

Fig. 6 shows the evolution of the thermal gain ΔT over time for different values of N while the remaining material parameters are fixed at their reference values of Table 1. The maximum thermal gain increases from 0.2 °C to 5.5 °C as the value of N decreases from 2.0 to 1.4. This increase is explained by the higher levels of liquid water capacity C_l, liquid water diffusivity D_l and volumetric heat capacity $(\rho c_p)_{eq}$ with reducing values of N (Table 3). In contrast, the adverse influence of higher thermal conductivity (Table 3) appears to be of lesser importance, at least for the case investigated here.

5.3. Hydraulic effusivity E

Section 3.1 has demonstrated that latent heat exchanges occur within earth walls through a condensation and liquid transport mechanism, primarily governed by the volumetric liquid water capacity C_l and the liquid water diffusivity D_l of the earth, while the vapour diffusivity D_v plays a secondary role. Drawing an analogy with thermal processes, it is intuitive to define hydraulic effusivity E $(kg/m^2 \sqrt{s})$ as a single parameter governing latent heat exchanges:

$$E = \sqrt{\rho_l D_l C_l} \tag{29}$$

This assumption is validated in Fig. 7a, which shows a good correlation between the maximum indoor thermal gain ΔT_{max} and the initial

value of hydraulic effusivity E within the earth wall for two sets of analyses. This correlation is observed for two sets of analyses where porosity n and the retention parameter N are varied individually, while all other parameters remain at their reference values from Table 1. The good correlation suggests that latent heat exchanges play a dominant role in determining the maximum indoor thermal gain ΔT_{max}. However, the difference between the two curves indicates a non-negligible impact from other physical processes governed by volumetric heat capacity and thermal conductivity, which are not included in the definition of hydraulic effusivity.

Finally, Fig. 7b shows the contour plot of the initial hydraulic effusivity E over the assumed ranges of porosity n and retention parameter N. Inspection of Fig. 7b indicates that the initial hydraulic effusivity E varies by five orders of magnitude attaining the highest value at the point where the porosity n is highest and the retention parameter N is smallest, which is also the point corresponding to the maximum thermal gain.

6. Comparison between earth and concrete walls

This section compares the hygrothermal performance of earth and concrete walls using the same model of the previous sections. The earth parameters are those of Table 1 while the concrete parameters are sourced from Künzel et al. [51]. Notably, the porosity is equal to 0.35 for earth and 0.155 for concrete.

Fig. 8 plots the hygrothermal properties of earth and concrete at different relative humidity levels over the range of interest. These properties have been calculated from the material parameters using the phase and constitutive relationships of Section 2. According to Fig. 8, earth walls outperform concrete walls in terms of considerably higher levels of liquid water diffusivity D_l and vapour diffusivity D_v, along with lower thermal conductivity, λ. Instead, concrete walls are superior to earth walls in terms of higher volumetric heat capacity, $(\rho c_p)_{eq}$ while the volumetric liquid water capacity, C_l is about equivalent in the two cases.

Fig. 9 confirms that earth walls are more efficient than concrete ones in delaying indoor thermal losses. Moreover, despite having significantly different material parameter values, concrete walls exhibit a response which closely mirrors that of earth walls when latent heat effects are neglected (Fig. 2). This observation indicates that the superior performance of earth walls is largely attributable to latent heat exchanges, due to the considerably higher liquid water diffusivity, while the influence of the other hygrothermal properties is less significant, at least for the case considered here.

Finally, Fig. 9 shows that, unlike earth walls, concrete walls maintain a virtually constant indoor relative humidity during the whole simulation period due to their relatively low liquid and vapour diffusivities.

7. Conclusions

A coupled finite element model has been developed to simulate the transfer of heat and water across earth walls, accounting for pore water phase changes and the associated latent heat fluxes. A simple one-dimensional analysis has been conducted to predict the hygrothermal changes inside an idealised room enclosed by two earth walls with infinite in-plane extension, which are exposed to a cold and humid external environment. The model requires a low number of parameters since the relevant hygrothermal properties are expressed as functions of the material porosity and water retention characteristics, facilitating parametric analyses. The main findings can be summarised as follow:

- Latent heat buffering by earth walls increases in the presence of greater gradients of relative humidity between the wet outdoor environment and the dry indoor space.
- Due to low vapor diffusivity, latent heat production is concentrated in the outer cold region of the wall, where pore vapor condensation
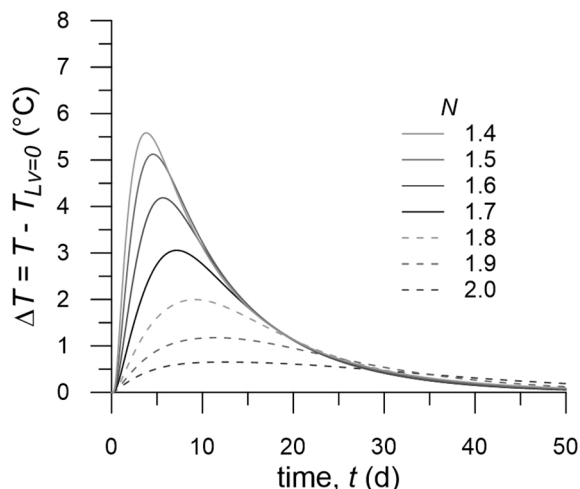

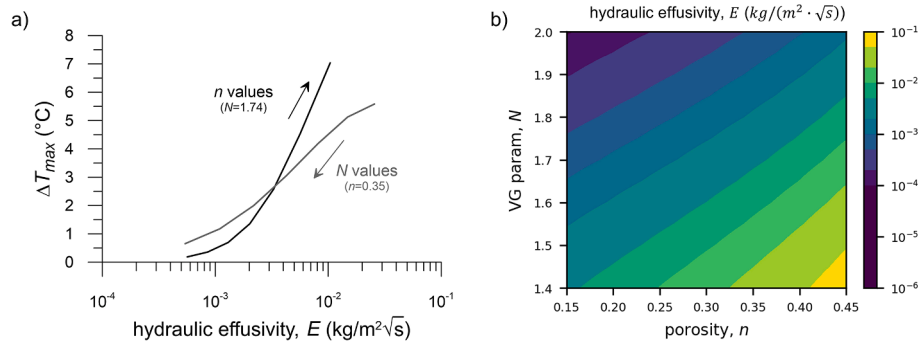**Fig. 6.** Thermal gain over time for different values of retention parameter N.

Fig. 7. a) Maximum thermal gain versus initial hydraulic effusivity E; b) Hydraulic effusivity E versus porosity n and Van Genuchten parameter N.
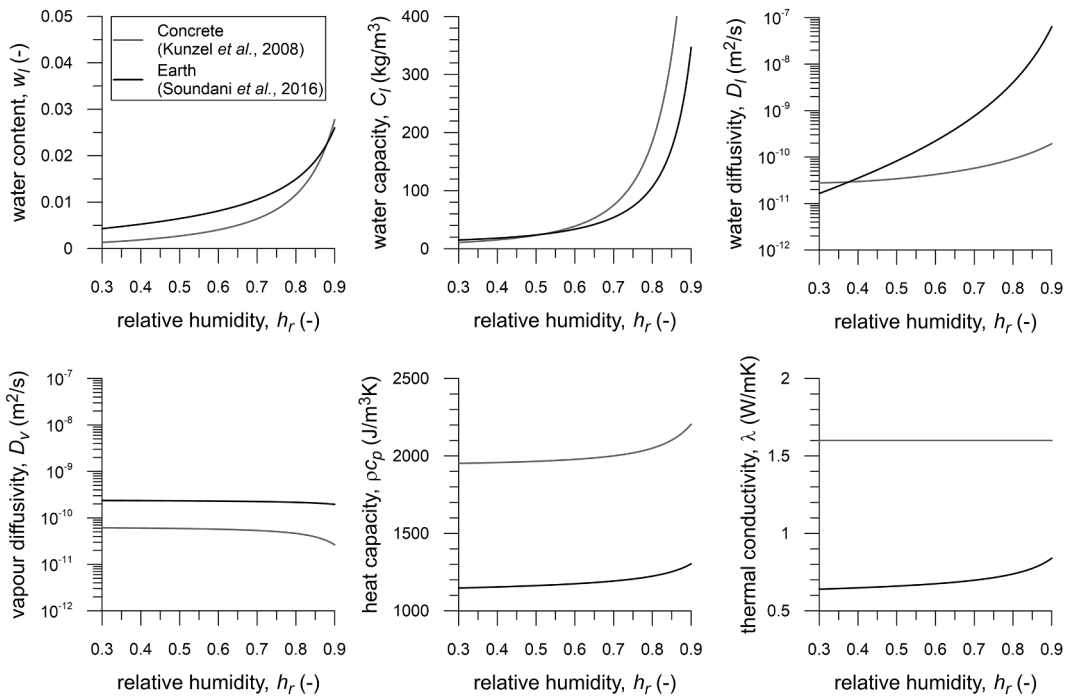

Fig. 8. Hygrothermal properties of earth and concrete walls at different relative humidity levels.
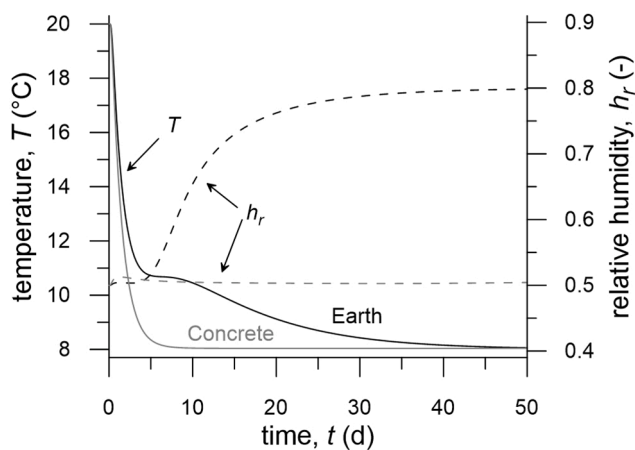

Fig. 9. Comparison of the hygrothermal performance of earth and concrete walls.

occurs. The condensed moisture is then transported in liquid form toward the inner region of the wall, where it evaporates back into the pore space. Additionally, a significant amount of latent heat is generated by water phase changes occurring at the outdoor and indoor wall faces. The total latent heat exchange from both the above contributions plays a crucial role in the high hygrothermal efficiency of earth walls.

- The mechanism of pore vapour condensation and inward liquid transport is magnified as the volumetric capacity and diffusivity of liquid water grow large. The volumetric capacity of liquid water increases with growing porosity and steepness of the retention curve while the diffusivity of liquid water increases with higher permeability, which in turn grows with larger porosity and degree of saturation. Latent heat exchanges are therefore maximised in highly porous walls that exhibit significant sensitivity of moisture content to ambient humidity, along with generally high saturation levels. These characteristics may however conflict with the structural requirement for relatively compact and dry perimeter walls, necessitating a careful balance between differing design demands.

- Analogous to thermal processes, hydraulic effusivity is defined as a function of both the volumetric capacity and diffusivity of liquid water, providing a single parameter that governs latent heat

exchanges. Larger values of hydraulic effusivity indicate a greater potential for latent heat buffering.

- The significance of latent heat exchanges is further highlighted by comparing the hygrothermal performance of earth and concrete walls. The lower thermal inertia of concrete walls parallels that of earth walls when the effect of latent heat transfers is switched off.

In conclusion, this study has investigated the fundamental hygrothermal performance of earthen walls under simple one-dimensional conditions for an idealised room without internal moisture and heat sources. These simple assumptions have provided a clearer theoretical understanding of the impact of latent heat transfers caused by pore water phase changes inside earth walls. However, one-dimensional models do not fully represent field applications and future research will focus on more realistic two- and three-dimensional models, considering indoor moisture and heat sources as well as actual meteorological data to define outdoor boundary conditions.

CRediT authorship contribution statement

Leonardo Maria Lalicata: Writing – original draft, Visualization, Validation, Software, Project administration, Methodology, Investigation, Formal analysis, Data curation, Conceptualization. **Agostino Walter Bruno:** Writing – review & editing. **Domenico Gallipoli:** Writing – review & editing, Supervision, Funding acquisition, Conceptualization.

Declaration of competing interest

The authors declare that they have no known competing financial interests or personal relationships that could have appeared to influence the work reported in this paper.

Acknowledgements

Data availability

Data will be made available on request.

References

[1] G. Minke, Earth Construction Handbook: The Building Material Earth in Modern Architecture, WIT Press; Computational Mechanics, 2000.

[2] J.C. Morel, A. Mesbah, M. Oggero, P. Walker, Building houses with local materials: Means to drastically reduce the environmental impact of construction, Build. Environ. 36 (10) (2001) 1119–1126, https://doi.org/10.1016/S0360-1323(00)00054-8.

[3] B. Little, T. Morton, Building with Earth in Scotland: Innovative Design and Sustainability, Scottish Executive Central Research Unit, Edinburgh, 2001.

[4] A. Arrigoni, C. Beckett, D. Ciancio, G. Dotelli, Life cycle analysis of environmental impact vs. durability of stabilised rammed earth, Constr. Build. Mater. 142 (2017) 128–136, https://doi.org/10.1016/j.conbuildmat.2017.03.066.

[5] A.W. Bruno, D. Gallipoli, C. Perlot, J. Mendes, Effect of stabilisation on mechanical properties, moisture buffering and water durability of hypercompacted earth, Constr. Build. Mater. 149 (2017) 733–740.

[6] A.W. Bruno, D. Gallipoli, C. Perlot, J. Mendes, Mechanical behaviour of hypercompacted earth for building construction, Mater. Struct. 50 (2) (2017) 160, https://doi.org/10.1617/s11527-017-1027-5.

[7] C.T.S. Beckett, R. Cardell-Oliver, D. Ciancio, C. Huebner, Measured and simulated thermal behaviour in rammed earth houses in a hot-arid climate. Part B: Comfort, J. Build. Eng. 13 (2017) 146–158, https://doi.org/10.1016/j.jobe.2017.07.013.

[8] J. Vyncke, L. Kupers, N. Denies, Earth as building Material – an overview of RILEM activities and recent Innovations in Geotechnics, MATEC Web Conf. 149 (2018) 02001, https://doi.org/10.1051/matecconf/201814902001.

[9] H. Anysz, P. Narloch, Designing the composition of cement stabilized rammed earth using artificial neural networks, Materials 12 (9) (2019) 1396, https://doi.org/10.3390/ma12091396.

[10] A.T. Nguyen, N.S.H. Truong, D. Rockwood, A.D. Tran Le, Studies on sustainable features of vernacular architecture in different regions across the world: a comprehensive synthesis and evaluation, Front. Archit. Res. 8 (4) (2019) 535–548, https://doi.org/10.1016/j.foar.2019.07.006.

[11] G. Cocco, G. Brando, E. Spacone, A review of local construction practices applied on unreinforced adobe buildings in South America, Front. Built Environ. 8 (2022) 974005, https://doi.org/10.3389/fbuil.2022.974005.

[12] J. Tan, J. Liang, L. Wan, B. Jiang, Influence of non-constant hygrothermal parameters on heat and moisture transfer in rammed earth walls, Buildings 12 (8) (2022) 1077, https://doi.org/10.3390/buildings12081077.

[13] D. Thompson, C. Augarde, J.P. Osorio, A review of current construction guidelines to inform the design of rammed earth houses in seismically active zones, J. Build. Eng. 54 (2022) 104666, https://doi.org/10.1016/j.jobe.2022.104666.

[14] A.E. Losini, T. Chitimbo, L. Létévé, M. Woloszyn, A.-C. Grillet, N. Prime, Hygrothermal characterization of rammed earth according to humidity variations, E3S Web Conf. 382 (2023) 23004, https://doi.org/10.1051/e3sconf/202338223004.

[15] A.E. Losini, M. Woloszyn, T. Chitimbo, A. Pelé-Peltier, S. Ouertani, R. Rémond, M. Doya, D. Gaillard, M.S. Force, J. Outin, A. Grillet, N. Prime, Extended hygrothermal characterization of unstabilized rammed earth for modern construction, Constr. Build. Mater. 409 (2023) 133904, https://doi.org/10.1016/j.conbuildmat.2023.133904.

[16] J.M.F. Pardo, Challenges and current research trends for vernacular architecture in a global world: a literature review, Buildings 13 (1) (2023) 162, https://doi.org/10.3390/buildings13010162.

[17] A.W. Bruno, L.M. Lalicata, R. Abdallah, A. Lagazzo, S. Arris-Roucan, F. McGregor, C. Perlot, D. Gallipoli, Synergic effect of hydrated lime and guar gum stabilisation on the mechanical, thermal and hygroscopic behaviour of a Ligurian earth material, Constr. Build. Mater. 439 (2024) 137258, https://doi.org/10.1016/j.conbuildmat.2024.137258.

[18] F. McGregor, A. Heath, A. Shea, M. Lawrence, The moisture buffering capacity of unfired clay masonry, Build. Environ. 82 (2014) 599–607.

[19] L. Soudani, A. Fabbri, J.-C. Morel, M. Woloszyn, P.-A. Chabriac, H. Wong, A.-C. Grillet, Assessment of the validity of some common assumptions in hygrothermal modeling of earth based materials, Energ. Build. 116 (2016) 498–511, https://doi.org/10.1016/j.enbuild.2016.01.025.

[20] P.M. Touré, V. Sambou, M. Faye, A. Thiam, M. Adj, D. Azilinon, Mechanical and hygrothermal properties of compressed stabilized earth bricks (CSEB), J. Build. Eng. 13 (2017) 266–271.

[21] T. Colinart, T. Vinceslas, H. Lenormand, A.H. De Menibus, E. Hamard, T. Lecompte, Hygrothermal properties of light-earth building materials, J. Build. Eng. 29 (2020) 101134.

[22] S.I. Kaitouni, M. Charai, N. Es-sakali, M.O. Mghazli, M. El Mankibi, S. Uk-Joo, M. Ahachad, J. Brigui, Energy and hygrothermal performance investigation and enhancement of rammed earth buildings in hot climates: from material to field measurements, Energ. Build. 315 (2024) 114325, https://doi.org/10.1016/j.enbuild.2024.114325.

[23] D. Allinson, M. Hall, Hygrothermal analysis of a stabilised rammed earth test building in the UK, Energ. Build. 42 (6) (2010) 845–852, https://doi.org/10.1016/j.enbuild.2009.12.005.

[24] F. Pacheco-Torgal, S. Jalali, Earth construction: lessons from the past for future eco-efficient construction, Constr. Build. Mater. 29 (2012) 512–519, https://doi.org/10.1016/j.conbuildmat.2011.10.054.

[25] F. McGregor, A. Heath, D. Maskell, A. Fabbri, J.-C. Morel, A review on the buffering capacity of earth building materials, Proc. Inst. Civil Eng. 169 (5) (2016) 241–251, https://doi.org/10.1680/jcoma.15.00035.

[26] D. Medjelekh, L. Ulmet, F. Dubois, Characterization of hygrothermal transfers in the unfired earth, Energy Proc. 139 (2017) 487–492, https://doi.org/10.1016/j.egypro.2017.11.242.

[27] L. Soudani, M. Woloszyn, A. Fabbri, J.-C. Morel, A.-C. Grillet, Energy evaluation of rammed earth walls using long term in-situ measurements, Sol. Energy 141 (2017) 70–80, https://doi.org/10.1016/j.solener.2016.11.002.

[28] A.W. Bruno, B. Scott, Y. D'Offay-Mancienne, C. Perlot, Recyclability, durability and water vapour adsorption of unstabilised and stabilised compressed earth bricks, Mater. Struct. 53 (6) (2020) 149, https://doi.org/10.1617/s11527-020-01585-7.

[29] A. Fabbri, J.-C. Morel, J.-E. Aubert, Q.-B. Bui, D. Gallipoli, B.V.V. Reddy, (A c c Di), Testing and Characterisation of Earth-based Building Materials and Elements: State-of-the-Art Report of the RILEM TC 274-TCE (vol. 35), 2022, Springer International Publishing. https://doi.org/10.1007/978-3-030-83297-1.

[30] G. Giuffrida, L. Ibos, A. Boudenne, H. Allam, Analysis of the thermal performances of uninsulated and bio-based insulated compressed earth blocks walls: from the material to the wall scale, J. Build. Eng. (2024) 109370.

[31] L. Ben-Alon, A.R. Rempel, Thermal comfort and passive survivability in earthen buildings, Build. Environ. 238 (2023) 110339, https://doi.org/10.1016/j.buildenv.2023.110339.

[32] F. Alassaad, K. Touati, D. Levacher, Y.E. Mendili, N. Sebaibi, Improvement of cob thermal inertia by latent heat storage and its implication on energy consumption, Constr. Build. Mater. 329 (2022) 127163, https://doi.org/10.1016/j.conbuildmat.2022.127163.

[33] F. Alassaad, K. Touati, D. Levacher, N. Sebaibi, Effect of latent heat storage on thermal comfort and energy consumption in lightweight earth-based housings, Build. Environ. 229 (2023) 109915, https://doi.org/10.1016/j.buildenv.2022.109915.

[34] L.M. Lalicata, A.W. Bruno, D. Gallipoli, A numerical insight into the hygrothermal buffering capacity of earthen building materials, Italian Geotech. J. 1 (2024) 11–24, https://doi.org/10.19199/2024.1.0557-1405.011.

[35] G. Guida, V.S. Vespo, G. Musso, G. Della Vecchia, The role of hydraulic and thermal properties of soil in evaporation: a numerical insight, Environ. Geotech. 1–18 (2023), https://doi.org/10.1680/jenge.22.00132.

[36] G. Musso, V.S. Vespo, G. Guida, G. Della Vecchia, Hydro-mechanical behaviour of a cement–bentonite mixture along evaporation and water-uptake controlled paths, Geomech. Energy Environ. 33 (2023) 100413, https://doi.org/10.1016/j.gete.2022.100413.

[37] H.M. Künzel, in: Simultaneous Heat and Moisture Transport in Building Components. One-and Two-Dimensional Calculation using Simple Parameters, IRB-Verlag Stuttgart, 1995, p. 65.

[38] F. Tariku, K. Kumaran, P. Fazio, Transient model for coupled heat, air and moisture transfer through multilayered porous media, Int. J. Heat Mass Transf. 53 (15) (2010) 3035–3044, https://doi.org/10.1016/j.ijheatmasstransfer.2010.03.024.

[39] ISO 24353, Hygrothermal Performance of Building Materials and Products Determination of Moisture Adsorption/Desorption Properties in Response to Humidity Variation, International Organization for Standardization, Geneva, Switzerland, 2008.

[40] M.T. van Genuchten, A closed-form equation for predicting the hydraulic conductivity of unsaturated soils, Soil Sci. Soc. Am. J. 44 (5) (1980) 892–898, https://doi.org/10.2136/sssaj1980.03615995004400050002x.

[41] L.M. Lalicata, A.W. Bruno, D. Gallipoli, Hygrothermal coupling in earth building materials, E3S Web Conf. 382 (2023) 23003, https://doi.org/10.1051/e3sconf/202338223003.

[42] Y. Mualem, A new model for predicting the hydraulic conductivity of unsaturated porous media, Water Resour. Res.. 12 (3) (1976) 513–522.

[43] X. Ren, Y. Zhao, Q. Deng, J. Kang, D. Li, D. Wang, A relation of hydraulic conductivity—void ratio for soils based on Kozeny-Carman equation, Eng. Geol. 213 (2016) 89–97, https://doi.org/10.1016/j.enggeo.2016.08.017.

[44] S.H. Lai, J.M. Tiedje, A.E. Erickson, In situ measurement of gas diffusion coefficient in soils, Soil Sci. Soc. Am. J. 40 (1) (1976) 3–6.

[45] B.A. Kimball, R.D. Jackson, R.J. Reginato, F.S. Nakayama, S.B. Idso, Comparison of field-measured and calculated soil-heat fluxes, Soil Sci. Soc. Am. J. 40 (1) (1976) 18–25, https://doi.org/10.2136/sssaj1976.03615995004000010010x.

[46] Lalicata, L.M., Bruno, A.W., Gallipoli, D., 2023. Hygrothermal modelling of earthen materials for building applications,in: A. Ferrari, M. Rosone, M. Ziccarelli, G. Gottardi (A c. Di), Geotechnical Engineering in the Digital and Technological Innovation Era, Springer Nature Switzerland, pp. 327–334. https://doi.org/10.1007/978-3-031-34761-0_40.

[47] A.E. Losini, A.-C. Grillet, L. Vo, G. Dotelli, M. Woloszyn, Biopolymers impact on hygrothermal properties of rammed earth: from material to building scale, Build. Environ. 233 (2023) 110087, https://doi.org/10.1016/j.buildenv.2023.110087.

[48] H. Cagnon, J.E. Aubert, M. Coutand, C. Magniont, Hygrothermal properties of earth bricks, Energ. Build. 80 (2014) 208–217, https://doi.org/10.1016/j.enbuild.2014.05.024.

[49] G. Giuffrida, R. Caponetto, F. Nocera, Hygrothermal properties of raw earth materials: a literature review, Sustainability 11 (19) (2019) 5342, https://doi.org/10.3390/su11195342.

[50] D. Gallipoli, A.W. Bruno, C. Perlot, J. Mendes, A geotechnical perspective of raw earth building, Acta Geotech. 12 (3) (2017) 463–478, https://doi.org/10.1007/s11440-016-0521-1.

[51] H.M. Künzel, A.H. Holm, M. Krus, I.H.M. Künzel, Hygrothermal properties and behaviour of concrete, WTA Almanach 1 (2008) 161–181.